Hindawi
Geofluids
Volume 2021, Article ID 6619440, 8 pages
https://doi.org/10.1155/2021/6619440

Research Article

Quantitative Study of Residual Oil Distribution during Water Flooding through Digital Core Analysis

Xuechao Liu[1,2] **Dazhong Ren**[2] **Fengjuan Dong**[2] **Junxiang Nan**[3] **and Ran Zhou**[4]

[1]*School of Mechanical and Electrical Engineering, Xi'an University of Architecture and Technology, Xi'an 710000, China*
[2]*Engineering Research Center of Development and Management for Low to Ultra-Low Permeability Oil & Gas Reservoirs in West China, Ministry of Education, Xi'an Shiyou University, Xi'an 710000, China*
[3]*Research Institute of Petroleum Exploration and Development, PetroChina Changqing Oilfield Company, Xi'an 710018, China*
[4]*Drilling and Production Technology Research Institute, CNPC Chuanqing Drilling Engineering Company Limited, Xi'an 710021, China*

Correspondence should be addressed to Xuechao Liu; chaochao27819@126.com

Received 28 December 2020; Revised 20 January 2021; Accepted 25 January 2021; Published 22 February 2021

Academic Editor: Feng Xiong

Copyright © 2021 Xuechao Liu et al. This is an open access article distributed under the Creative Commons Attribution License, which permits unrestricted use, distribution, and reproduction in any medium, provided the original work is properly cited.

The character of residual oil formed during water flooding, one important technique to enhance oil recovery, is helpful to further study permeability and recovery in tight sandstone oil reservoirs. In this paper, we take a tight sandstone reservoir in Ordos Basin as the research object and use in situ displacement X-CT scanning technology to analyze the dynamic characteristics of oil during water flooding. Firstly, core pore radius and oil storage space radius were measured from digital cores which are acquired in different water flooding stages by X-CT scanning technology. Secondly, analytical and evaluation methods were established to describe fluid distribution in the pore space of the core in different water flooding stages based on curve similarity. Finally, by numerical results, we analyzed the oil distribution features in the process of water flooding for core samples. In this paper, the oil distribution characteristics during water flooding are revealed based on digital core analysis. Also, a quantitative evaluation method is given to provide theoretical guidance.

1. Introduction

Crude oil is one of the most important energy sources. Nowadays, more and more advanced and low-cost development technologies are needed to enhance reservoir recovery [1]. Water flooding and other enhanced oil recovery techniques are based on the common methodology aimed at increasing oil production; however, it is usually with high cost [2, 3]. Therefore, petroleum engineering methods and numerical simulation are needed to understand oil mobility and distribution characteristics, which are also needed to simulate reservoir history and predict future performance [4, 5]. It would make the development process more rational. However, due to reservoir characteristics, both the pore structure and oil distribution are complicated. Besides, the conventional microscope observation method is not enough to analyze the real core, so that other techniques, like X-ray computed tomography, are needed for quantitative and detailed description on the microscale. In 1991, X-ray computed tomography (X-CT) technology was introduced for porous media analysis. It can provide lossless images at micrometer or even nanometer scale, which makes microscale analysis possible and has become one of the effective means in oil reservoir studies [6–10].

In recent years, researchers have performed X-CT scans on real cores to obtain images and reconstruct the pore structure to analyze reservoir characteristics [11–14], seepage simulation, and enhanced oil recovery [15, 16]. Combining with the image processing method, X-CT scanning technology also extracts the distribution of different fluids in a core, so as to study pore structure and fluid motion [17–19]. Using this technique, some researchers have further studied the pattern and quantity of liquid clustering in real core samples [20]. For reservoir studies, some researchers have observed the distribution of remaining oil in different flow states (including oil-water system and immiscible CO_2 brine

system) [21–24]. With in situ displacement, An et al. have found volume of residual oil can also be quantitatively calculated and classified with shape factor [25]. In addition, other researchers have found different patterns of residual water and their effect on permeability through digital core analysis [26].

However, there are few researches that focus on the relationship between oil distribution and pore size in the process of displacement based on digital core analysis. In this paper, we studied the relationship between oil distribution and pore radius during the process of water flooding by using in situ displacement scanning technique for tight sandstone. We take the Chang 7 tight sandstone reservoir in Ordos Basin as the research object and use in situ displacement scanning technology to deeply analyze dynamic change characteristics of oil in different pore sizes during water flooding.

2. Experiment

The research object is from Chang 7 reservoir in Huaqing oilfield, Ordos Basin, China, with a length of 5 mm and a diameter of 3 mm. The device comprises a low-rate fluid injection system and in situ displacement system equipped with X-CT scanning system (510 VERSA, made by Carl Zeiss Optics Co. Ltd.). We set the resolution of the scanning equipment at 3.32 μm per pixel, and the 3D reconstruction volume comprised $1004 \times 1004 \times 1005$ pixels. Confining pressure was configured at 2.0 MPa, displacement pressure was constant at 0.02 MPa, and the room temperature was 25°C. The 10% potassium iodide solution was used as saturated fluid to improve the imaging ability of water. The experimental steps are as follows:

(1) Clean oil and salt from the core with distilled water, then conduct porosity and permeability tests

(2) Scan the core in dry situation for 14 hours

(3) Saturate the core with potassium iodide solution to get a saturated water situation and scan for 14 hours

(4) Saturate the core with oil to get a saturated oil situation and scan for 14 hours

(5) Saturate the core with potassium iodide solution to get a residual oil situation and scan for 14 hours

(6) Extract and process data acquired from X-CT scanning results

3. Digital Core Results and Analysis

3.1. Scanning Results. Scanning slices of the core in the water flooding procedure are shown in Figure 1. According to X-ray attenuation when penetrating different materials, the dark gray range below the low threshold indicates pores and oil, and the light gray range above the high threshold indicates water. In Figure 1(b), bound water fills in small pores of the core, while existing in the corners or similar membranes in large-scale pores. In Figure 1(c), after water flooding, bound water fills most of pores, and large-size pores are filled with oil and water.

From these scanning slices, the pore and water phase can be extracted by image processing. Before image segmentation, nonlocal mean algorithm was used to filter noise [27, 28]. Then, a watershed algorithm was employed to segment the rock matrix, water phase, and gas phase based on different thresholds. By logical operation, we reconstructed the oil and water volume from the pore structure in a dry situation and the water phase in a saturated situation, as shown in Figure 2. Compared with saturated oil, the water content in the core of the residual oil state extremely increased, but residual oil also exists.

A local core, with a central position of (356, 125, 228) and a size of $420 * 270 * 154\,\mu$m, is extracted as shown in Figure 3. We can observe more detail about the oil-water distribution changing during water flooding.

In Figure 3(a), the local core contains large-size and small-size pores with narrow throats. After water flooding in Figure 3(e), there is a large amount of residual oil in the large pores, while the small pores are filled with water. The reason is that the internal pore throat is narrow due to heterogeneity. That results in oil flow truncation and the residual oil enrichment in macropores. At the same time, a fingering phenomenon also occurs and makes it difficult for the oil to flow in the macropore, so that only part of the oil in the outermost layer of the oil phase is driven away.

3.2. Measurement Results. Figure 4 shows the composition of porosity, oil saturation, and water saturation extracted from the digital core, which are consistent with the experimental measurements. In the saturated oil situation, oil saturation is lower than water saturation, mainly because there are narrow throats and part of the pore space cannot be filled by oil during saturation of the core with oil. However, after water flooding, oil saturation substantially reduces. Oil displacement efficiency is 66.28%, indicating that the oil displacement is efficient. Combined with Figure 3, the reason is that oil in small-size pores of the core is driven out efficiently.

4. Displacement Evaluation Based on Curve Similarity

With the digital core, we use curve similarity to calculate difference of the distribution between the pore and every stage during water flooding and describe the dynamic distribution character.

4.1. Evaluation Model. Figure 5 describes the probability accumulation distribution of the radius for the porosity and oil phase in different states.

These three curves have the same trend, but their difference reflected in the influence on oil distribution is caused by the pore structure.

Similarity is a research hotspot in the data mining field. By measuring the similarity degree and analyzing the association between the objects, it provides guidance for research in different fields [29, 30]. In this paper, the displacement evaluation system based on similarity is established which

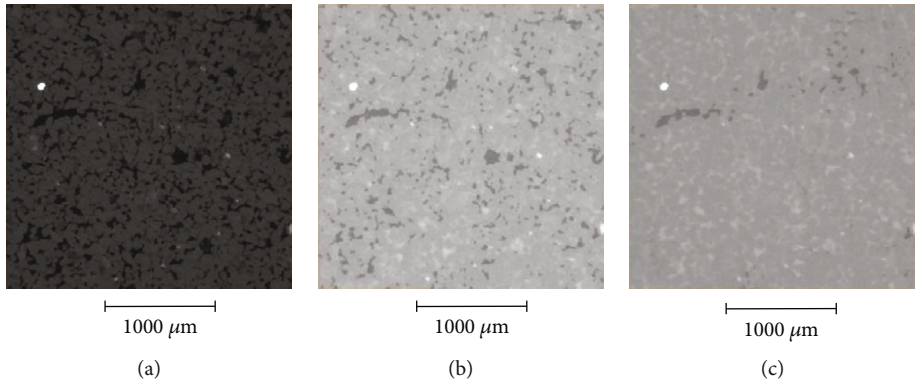

Figure 1: Scanning slices of the core: (a) dry situation, (b) saturated oil situation, and (c) residual oil situation.

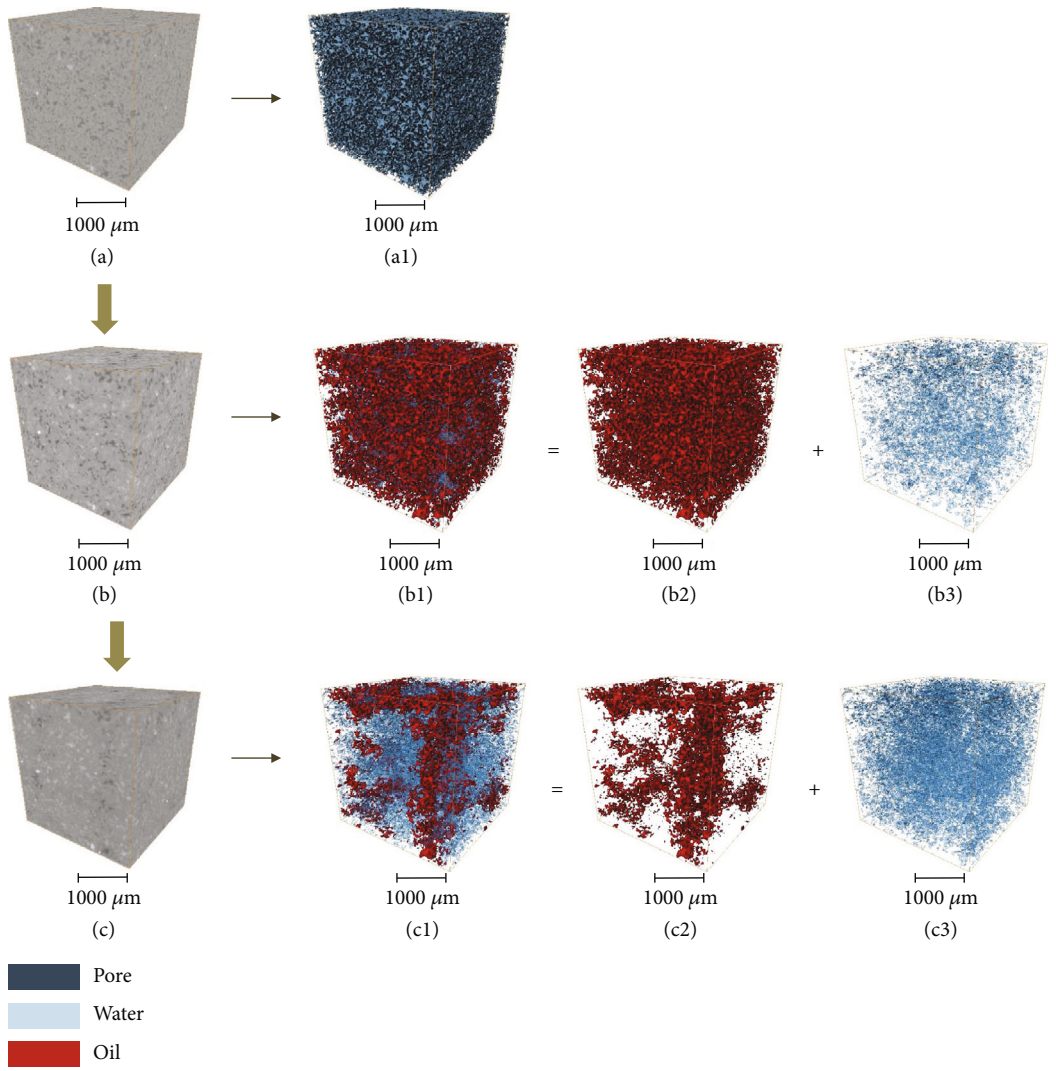

Figure 2: The core, oil, and water volume in different situations: (a) dry situation, (b) saturated oil situation, and (c) residual oil situation.

includes three indicator—overall trend, translation, and retractility, as shown in Figure 6.

Firstly, the radius of the porosity and oil phase in the saturated oil situation and residual situation is extracted. Secondly, frequency cumulative distribution curve of parameters is constructed after parameter normalization. Finally, the curve similarity is analyzed with three indicators based on evaluation results of displacement. The overall trend should be combined with saturation to analyze displacement efficiency and oil movement features in pores. The retractility

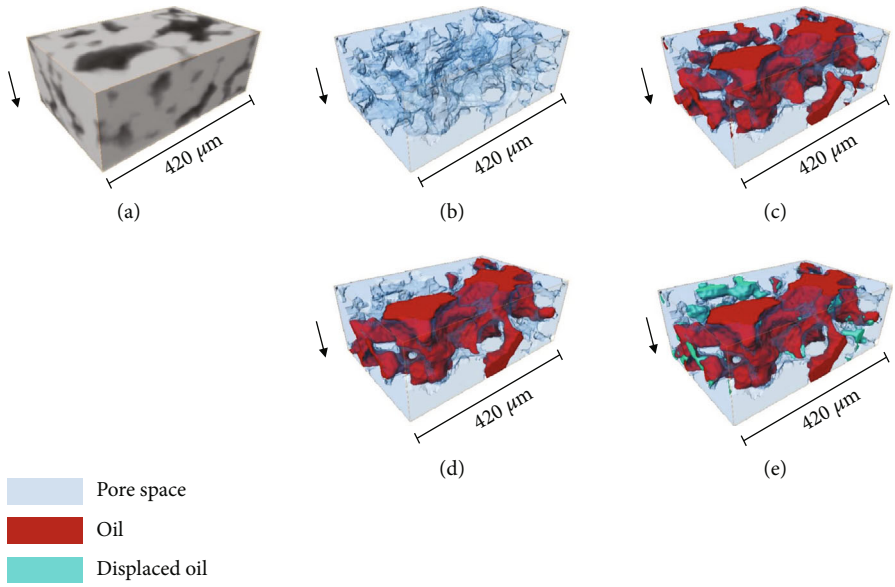

Figure 3: Oil and water distribution in the local core: (a) dry situation, (b) pore structure, (c) saturated oil situation, (d) residual oil situation, and (e) changing of oil distribution.

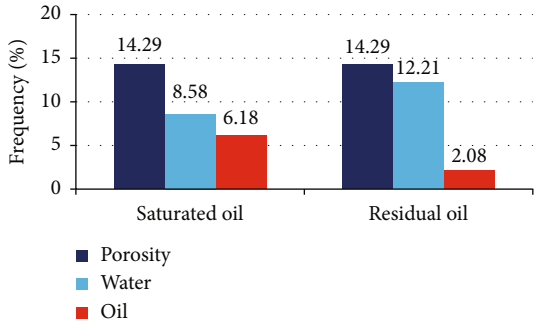

Figure 4: Saturation comparison.

describes the relation between different pore radii and oil changing rates. The translation reflects relative distribution of residual oil in pore space.

4.2. Evaluation Index

4.2.1. Data Specification. The heterogeneity leads to diversity of the pore structure in the core. Therefore, only by standardizing parameters can the evaluation index have generalization ability. The normalization equation can

$$y_i = \min_{1<j\le n}\{y_j\} + \frac{x_i - X_{\min}}{X_{\max} - X_{\min}} \cdot \left(\max_{1<j\le n}\{y_j\} - \min_{1<j\le n}\{y_j\}\right), \tag{1}$$

be expressed as follows: where x_i is data to be normalized and $i \in (1, n)$, n is number of samples, y_i is the normalized data, $X_{\min}$ and $X_{\max}$ are the actual radius range, and $\max_{1<j\le n}\{y_j\}$ and $\min_{1<j\le n}\{y_j\}$ are the data range after normalization. In the water flooding procedure, the radius range of the oil phase changes under different states, so the porosity parameter in the dry situation is taken as the standard reference. In this study, the pore radius range of the core in a dry situation is 3.38 μm-810 μm. Hence, $X_{\min}$ and $X_{\max}$ are set to 3.38 μm and 810 μm, $\min_{1<j\le n}\{y_j\}$ is set to 1, and $\max_{1<j\le n}\{y_j\}$ is set to 1000.

4.2.2. Overall Trend. Since cumulative distributions are similar in different core situations, the overall trend is calculated by absolute value difference between the evaluated curve and the reference curve. Ideally, pores in the core should be filled with oil and the oil should be completely displaced. Therefore, the reference curve

$$F = \frac{\sum_{i=0}^{n} |y_i^S - y_i^D| \cdot y_{ir}}{n}, \tag{2}$$

in this paper is the distribution curves of the core in the dry situation. The overall trend is defined as follows: where i is the sampling point of the pore radius, n is the total number of sampling points, y_i^S is the value of the cumulative distribution corresponding to the i sampling point in the reference curve, y_i^D is the value of the cumulative distribution corresponding to the i sampling point in the evaluated curve, and y_{ir} is the aperture coordinate.

4.2.3. Retractility. The coordinate of the pore radius is divided into sections, and the maximum difference is used to describe the horizontal retractility for every section with the help of the deviation standardization idea. It is defined via the following equation:

$$e_j = 1 - \frac{y_{j_{\max}}^D - y_{j_{\min}}^D}{y_{j_{\max}}^S - y_{j_{\min}}^S + 0.01}, \tag{3}$$

where $y_{j_{\max}}^S$ and $y_{j_{\min}}^S$ are the max value and min value in

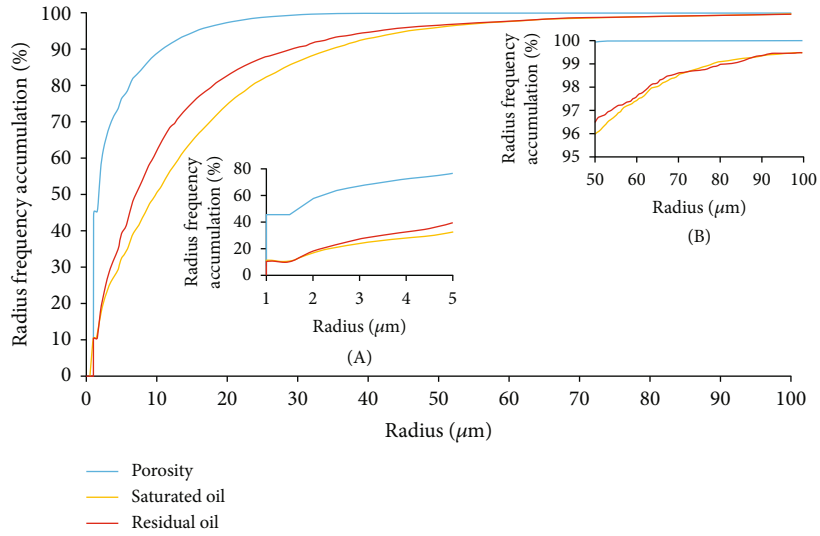

Figure 5: Probability accumulation curve of pore distribution under different states (dry sample, saturated oil, and residual oil): (A) cumulative distribution of pore radius from 1 μm to 5 μm; (B) cumulative distribution of pore radius from 50 μm to 100 μm.

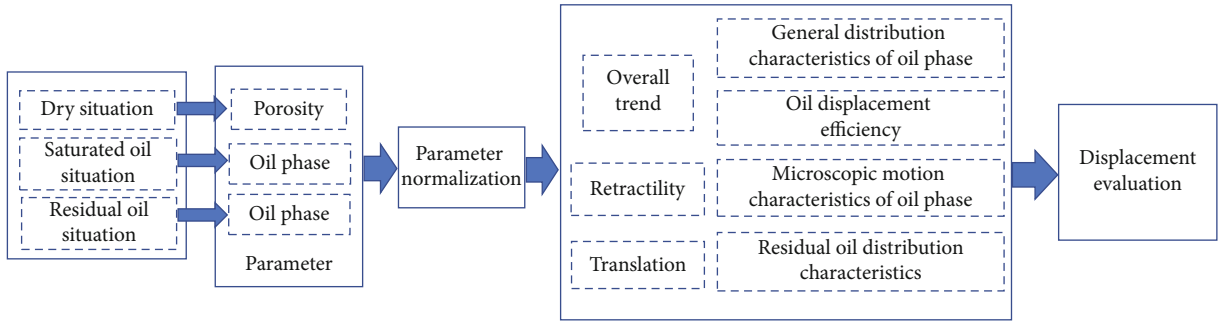

Figure 6: Water flooding description model.

section j of the reference curve, $y^D_{j_{\max}}$ and $y^D_{j_{\min}}$ are the max value and min value in section j of the evaluated curve, and k is number of sections. We add 0.01 to the denominator to prevent the denominator from being 0.

During flooding, when movable oil in the pore moves, the radius of the oil space changes, following the corresponding statistical distribution curve change, which reflects retractility. The greater the absolute value of retractility, the more the variation of the movable oil in the space range.

We also need to set an appropriate step size to accurately reflect the relationship between the pore radius and movable oil. If the step size is too large, it is impossible to obtain accurate calculation results; if the step size is too small, the results cannot be calculated. In this paper, the step size is 10 μm.

According to formula (3), the retractility degree under different aperture ranges is calculated as $E = (e_1, \cdots, e_j, \cdots, e_k)$.

4.2.4. Translation Measurement. There are two aspects to translation, the horizontal and vertical differences. Since the longitudinal range of the curve is constant between 0% and 100%, horizontal differences are mainly evaluated.

$$L_h = \frac{\sum_{j=1}^{N}\sum_{i=1}^{m}\left(y^D_{\max_{ji}} - y^S_{\max_{ji}}\right)}{N}. \quad (4)$$

The formula is shown in Equation (4), where m is the sampling number of the pore radius in the sublevel interval, N is the number of segments, $y^D_{\max_{ji}}$ is the ith big radius in the j section for the curve to be evaluated, and $y^S_{\max_{ji}}$ is the i th big radius in the j section for reference curve. In this paper, 10% is taken as the step size and then $N = 10$.

4.3. Water Flooding Analysis Based on Similarity. The calculation results of the overall trend, retractility, and translation based on curve similarity are shown in Figure 7. The dry situation porosity is the reference curve in "dry sample-saturated oil" and "dry sample-residual oil."

In Figure 7(a), the overall trend difference of the oil phase between the dry situation and the saturated oil is valued at 33, showing that oil in the saturated oil state accounts for more in the macrospore space. Combined with Figure 5, it again indicates that the pore space is not filled by oil due to the pore end or narrow throat when that is

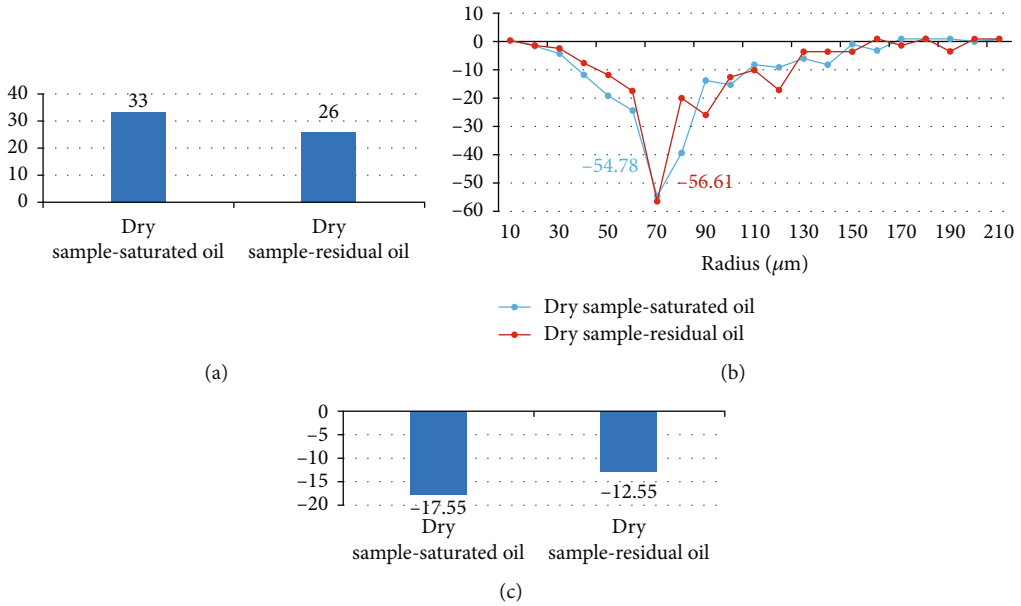

FIGURE 7: Water flooding evaluation results by curve similarity: (a) results of overall trend, (b) results of retractility, and (c) results of translation.

saturated by oil. Overall trend difference between the dry sample and the residual oil is 26, revealing that oil in large pores is partly expelled after oil flooding, which increases the proportion of oil in small pores.

In Figure 7(b), the minimum retractility value is obtained within the aperture range of 60 μm-70 μm (actual core aperture is 51 μm-59 μm). According to the inverse process of Equation (1), it indicates that the oil moved greatly with the pore radius in this range during water flooding, while, in those pores with a radius greater than 210 μm (real size is 172 μm) or less than 10 μm (real size is 10.64 μm), the retractility result tends to be 0, showing that little oil changed in those areas. It also reflects that oil in pores with a large size in our study sample is not easy to move, and pores with a small size cannot be filled.

In Figure 7(c), compared with the dry sample, saturated oil gets a translation degree at -17.55 and curve has shifted to the right corresponding to the oil moving in large pores. The displacement degree of the residual oil is -12.55, absolutely less than 17.55, also indicating oil moving in large pores.

The conclusions of these three indexes are consistent and quantitatively show microscopic movement of oil in pores during water flooding.

5. Conclusion

In this paper, we take the tight sandstone in Ordos Basin as the research object, use in situ displacement scanning technology to conduct a water flooding experiment and employ image processing to extract digital cores. Then, a water flooding evaluation model is established by curve similarity analysis.

(1) We extract the digital core based on an in situ displacement scan and observe the dynamic distribution of oil during water flooding. And then, we calculate the oil saturation, water saturation, and probability cumulative distribution of the core aperture

(2) Based on the curve similarity, the displacement evaluation model is established: the displacement efficiency is analyzed by the overall trend, the relation between the oil momentum and the pore diameter is described by the retractility degree, and the distribution characteristic of oil is reflected by the translation degree. At the same time, the normalization method is given to improve the generalization

(3) According to the calculated results, we describe the difference of fluid distribution in the pore space of the core under different states during displacement. This model further explains the dynamic change rule of oil occurring in the process of displacement, provides a quantifiable comparative analysis for reservoir study in the same area, and gives theoretical guidance for reservoir development by water driving

Data Availability

The experimental data belongs to the laboratory, Engineering Research Center of Development and Management for Low to Ultra-Low Permeability Oil & Gas Reservoirs in West China, Ministry of Education, Xi'an Shiyou University. The readers can obtain the data if permitted.

Conflicts of Interest

The authors declare that no conflicts of interest exit regarding the submission of this paper.

Acknowledgments

This study was supported by the Open Funds of Engineering Research Center of Development and Management for Low to Ultra-Low Permeability Oil & Gas Reservoirs in West China (no. KFJJ-XB-2020-3), National Natural Science Foundation of China (nos. 41702146 and 51934005), Open Fund of Shaanxi Key Laboratory of Advanced Stimulation Technology for Oil & Gas Reservoirs (no. 20JS120), Young Science and Technology Talents Foundation of Shanxi Province (no. 2019KJXX-054), Natural Science Foundation of Shaanxi Provincial Department of Science and Technology (no. 2019JM-286), Doctoral Research Initiation Fund (no. 6040300529), and Youth Foundation of Xi'an University of Architecture and Technology (no. 6040517045).

References

[1] R. Bondia, S. Ghosh, and K. Kanjilal, "International crude oil prices and the stock prices of clean energy and technology companies: evidence from non-linear cointegration tests with unknown structural breaks," *Energy*, vol. 101, pp. 558–565, 2016.

[2] Z. Li, H. Liu, Z. Dun, L. Ren, and J. Fang, "Grouting effect on rock fracture using shear and seepage assessment," *Construction and Building Materials*, vol. 242, article 118131, 2020.

[3] P. Bahrami, P. Kazemi, S. Mahdavi, and H. Ghobadi, "A novel approach for modeling and optimization of surfactant/polymer flooding based on genetic programming evolutionary algorithm," *Fuel*, vol. 179, pp. 289–298, 2016.

[4] Z. Li, S. Liu, W. Ren, J. Fang, Q. Zhu, and Z. Dun, "Multiscale laboratory study and numerical analysis of water-weakening effect on shale," *Advances in Materials Science and Engineering*, vol. 2020, Article ID 5263431, 14 pages, 2020.

[5] S. Berg, R. Armstrong, A. Georgiadis et al., "Onset of oil mobilization and nonwettingphase cluster-size distribution," *Petrophysics*, vol. 56, no. 1, pp. 15–22, 2015.

[6] H. Wang, R. Rezaee, and A. Saeedi, "Evaporation process and pore size distribution in tight sandstones: a study using NMR and MICP," *Procedia Earth and Planetary Science*, vol. 15, pp. 767–773, 2015.

[7] C. Zhu, M. C. He, Q. Yin, and X. H. Zhang, "Numerical simulation of rockfalls colliding with a gravel cushion with varying thicknesses and particle sizes," *Geomechanics and Geophysics for Geo-Energy and Geo-Resources*, vol. 7, no. 1, p. 11, 2021.

[8] C. Zhu, X. D. Xu, W. R. Liu et al., "Softening damage analysis of gypsum rock with water immersion time based on laboratory experiment," *IEEE Access*, vol. 7, pp. 125575–125585, 2019.

[9] G. Tysarczyk-Niemeyer, M. Steffens, and H. Schiessl, "The XCT 1000M: validation of a new peripheral quantitative computed tomograph for mice measurements," *Bone*, vol. 19, no. 3, pp. 164–164, 1996.

[10] H. Sun, H. Belhaj, G. Tao, S. Vega, and L. Liu, "Rock properties evaluation for carbonate reservoir characterization with multiscale digital rock images," *Journal of Petroleum Science and Engineering*, vol. 175, pp. 654–664, 2019.

[11] Y. Wang, B. Zhang, S. H. Gao, and C. H. Li, "Investigation on the effect of freeze-thaw on fracture mode classification in marble subjected to multi-level cyclic loads," *Theoretical and Applied Fracture Mechanics*, vol. 111, article 102847, 2021.

[12] C. Zhu, M. C. He, M. Karakus, X. B. Cui, and Z. G. Tao, "Investigating toppling failure mechanism of anti-dip layered slope due to excavation by physical modelling," *Rock Mechanics and Rock Engineering*, vol. 53, no. 11, pp. 5029–5050, 2020.

[13] X. Zhao, M. Blunt, and J. Yao, "Pore-scale modeling: effects of wettability on waterflood oil recovery," *Journal of Petroleum Science and Engineering*, vol. 71, no. 3–4, pp. 169–178, 2010.

[14] K. Singh, R. Niven, T. Senden et al., "Remobilization of residual non-aqueous phase liquid in porous media by freeze-thaw cycles," *Environmental Science & Technology*, vol. 45, no. 8, pp. 3473–3478, 2011.

[15] D. Ren, H. Huang, J. Qi, and P. Zheng, "One-pot template-free cross-linking synthesis of SiO_x–SnO_2@C hollow spheres as a high volumetric capacity anode for lithium-ion batteries," *Energy Technology*, vol. 8, no. 7, article 2000314, 2020.

[16] W. J. McLendon, P. Koronaios, R. Enick et al., "Assessment of CO_2-soluble non-ionic surfactants for mobility reduction using mobility measurements and CT imaging," *Journal of Petroleum Science and Engineering*, vol. 119, no. 3, pp. 196–209, 2014.

[17] C. Zhu, Z. H. Yan, Y. Lin, F. Xiong, and Z. Tao, "Design and application of a monitoring system for a deep railway foundation pit project," *IEEE Access*, vol. 7, pp. 107591–107601, 2019.

[18] H. Geistlinger, S. Mohammadian, S. Schlueter, and H. Vogel, "Quantification of capillary trapping of gas clusters using X-ray microtomography," *Water Resources Research*, vol. 50, no. 5, pp. 4514–4529, 2014.

[19] Z. T. Karpyn, M. Piri, and G. Singh, "Experimental investigation of trapped oil clusters in a water-wet bead pack using X-ray micro tomography," *Water Resources Research*, vol. 46, no. 4, pp. 475–478, 2010.

[20] S. Iglauer, M. Fernø, P. Shearing, and M. Blunt, "Comparison of residual oil cluster size distribution, morphology and saturation in oil-wet and water-wet sandstone," *Journal of Colloid and Interface Science*, vol. 375, no. 1, pp. 187–192, 2012.

[21] M. Andrew, B. Bijeljic, and M. Blunt, "Pore-by-pore capillary pressure measurements using X-ray microtomography at reservoir conditions: curvature, snap-off, and remobilization of residual CO_2," *Water Resources Research*, vol. 50, no. 11, pp. 8760–8774, 2014.

[22] C. Guo, X. Wang, H. Wang, S. He, H. Liu, and P. Zhu, "Effect of pore structure on displacement efficiency and oil-cluster morphology by using micro computed tomography (μCT) technique," *Fuel*, vol. 230, pp. 430–439, 2018.

[23] D. Yin, S. Chen, Y. Ge, and R. Liu, "Mechanical properties of rock-coal bi-material samples with different lithologies under uniaxial loading," *Journal of Materials Research and Technology*, vol. 10, pp. 322–338, 2021.

[24] X. Gu, C. Pu, H. Huang et al., "The visual and quantitative study of the microoccurrence of irreducible water at the pore and throat system in a low-permeability sandstone reservoir by using microcomputerized tomography," *Geofluids*, vol. 2018, Article ID 6062475, 14 pages, 2018.

[25] S. An, J. Yao, Y. Yang, W. Zhang, J. Zhao, and A. Li, "The microscale analysis of reverse displacement based on digital core," *Journal of Natural Gas Science and Engineering*, vol. 40, pp. 138–144, 2017.

[26] Q. Lei, L. Zhang, H. Tang, Y. Zhao, M. Chen, and C. Xie, "Quantitative study of different patterns of microscale residual water and their effect on gas permeability through digital core

analysis," *Journal of Petroleum Science and Engineering*, vol. 196, article 108053, 2020.

[27] Q. Meng, H. Wang, M. Cai, W. Xu, X. Zhuang, and T. Rabczuk, "Three-dimensional mesoscale computational modeling of soil-rock mixtures with concave particles," *Engineering Geology*, vol. 277, article 105802, 2020.

[28] A. Buades, B. Coll, and J. M. Morel, "A non-local algorithm for image denoising," in *2005 IEEE Computer Society Conference on Computer Vision and Pattern Recognition (CVPR'05)*, pp. 60–65, San Diego, CA, USA, June 2005.

[29] D. Ren, D. Khadjiev, and M. Peken, "Identifications of paths and curves under the plane similarity transformations and their applications to mechanics," *Journal of Geometry and Physics*, vol. 151, article 103619, 2020.

[30] J. G. Alcázar, C. Hermoso, and G. Muntingh, "Detecting similarity of rational plane curves," *Journal of Computational and Applied Mathematics*, vol. 269, pp. 1–13, 2014.